Civil Engineering Infrastructures Journal 2025, 58(2): 419-427
DOI: 10.22059/ceij.2024.364855.1957

TECHNICAL NOTES

Permeable Triangular Vanes Effect on Turbulent Flow Field

Ahmadi Adli, S.[1], Abbaspour, A.[2*], Hosseinzadeh Dalir, A.[3] and Parsa, J.[2]

[1] Ph.D., Department of Water Science and Engineering, Faculty of Agriculture, University of Tabriz, Tabriz, Iran.
[2] Associate Professor, Department of Water Science and Engineering, Faculty of Agriculture, University of Tabriz, Tabriz, Iran.
[3] Professor, Department of Water Science and Engineering, Faculty of Agriculture, University of Tabriz, Tabriz, Iran.

Received: 05 Sep. 2023; Revised: 8 May 2024; Accepted: 10 Jun. 2024

ABSTRACT: In this study, a Large Eddy Simulation (LES) model was used to simulate the turbulent flow field around the triangular vanes affected by different permeability rates and vanes angle. Depth-averaged velocity and bed shear stress distributions are affected due to the local effects of the triangular vanes structure; however, by increasing the permeability rate, these structures impacts on the flow field have been reduced. On average, maximum bed shear stress values around the simulated vanes were 3.47 times the τ_{Mean}. Tip velocity near the bed region for the 70% permeable vane with $\theta = 58°$ and $\theta = 68°$ was 1.13 times the V_{app}. The thalweg line alignment was affected by the flow field constriction and local flow structure. Due to the triangular vanes' cross-sectional opening and smoother flow deflection, which varied between 4º and 30º, the thalweg line generally showed a minor deflection from the channel centerline.

Keywords: Large Eddy Simulation, Permeability, Triangular Vanes, Turbulent Flow, Vanes Angle.

1. Introduction

In recent years, new river restoration techniques such as bank-attached triangular vanes have been proposed not only to protect river banks and stabilize the river bed but also to improve the river ecosystem regarding the growing awareness of the environmental issues (Pagliara and Kurdistani, 2017).

Bhuiyan et al. (2010) studied the effect of bank-attached triangular vanes on flow pattern and bed topography variations in the large-scale meandering channel. They concluded that the induction of a secondary flow near the outer bank counteracts the main spiral flow in the bend, and horizontal vortices are not formed behind these structures. Kang et al. (2011) investigated the effect of the different geometry and permeability rates on turbulent flow characteristics around the rectangular and triangular-shaped groins. Generally, they concluded that weaker vortices occurred around triangular-shaped groins, and these structures are appropriate for multipurpose design. Teraguchi et al. (2011) studied the scour-deposition process and flow characteristics affected by permeable and impermeable groins. Results showed that velocity has been decreased around permeable groins, and the absence of strong

* Corresponding author E-mail: akabbaspour@yahoo.com

eddies around these structures prevents excessive siltation. Fang et al. (2014) employed a Large Eddy Simulation (LES) model to study the effect of groin head shape, aspect ratio, and length on flow characteristics around non-submerged groin in a shallow open channel flow.

Bahrami Yarahmadi and Shafai Bejestan (2015) studied scour-deposition and flow patterns affected by different triangular vane spacing in a 90° mild flume bend. Results showed that due to the vanes presence in the channel, counter-clockwise secondary flow near the outer bank forms, which counteracts the clockwise main secondary flow along the bend. Ferro et al. (2019) proposed a new technique, which is a combination of a permeable groin and a triangular vane, and they evaluated the effectiveness of this technique in river bends. Different combinations and flow rates were considered in this study. Results showed that the triangular vane enhances the performance of the permeable groin. Wang et al. (2020) investigated turbulent flow features in the wide and narrow channels using an Acoustic Doppler Velocimeter (ADV). In this study, turbulent kinetic energy, Reynolds shear stress, and turbulent intensities were investigated. Shampa et al. (2020) focused on the effects of the different installation angles and spur dikes position on three-dimensional flow characteristics. Three-dimensional velocity variations, flow depth fluctuations, and bed shear stress distribution were analysed to evaluate the efficiency of these structures.

Abdou et al. (2021) used LES to study flow characteristics in a 193° sharp laboratory flume bend. Water depth fluctuations, stream wise and transverse velocity distributions at different sections and over the whole channel were investigated. Iqbal et al. (2021) used Fluent model and Reynolds Stress Model (RSM) to study velocity profiles, turbulent intensities, and turbulent kinetic energy at different selected points in the horizontal plane around permeable rectangular spur dikes. Results showed that strong turbulent flows do not occur around the tip region of the permeable spur dikes, and turbulent flow features have been decreased around these structures. Jafari and Sui (2021) studied turbulence structure and velocity variations around the non-submerged spur dikes having different orientation angles under the ice covered conditions using ADV. Results showed that tip region was critical and strong velocity fluctuations mainly occurred in this region, also ice cover on the water surface affects the bed shear stress and turbulence intensities. Haider et al. (2022) used Fluent to study the turbulent flow characteristics affected by the permeable spur dikes with different staggered pores having varying angles. Different permeability rates and staggered pores angles were considered. Velocity distributions, turbulent kinetic energy, turbulence intensity, and wall shear stress were compared around the considered permeable spur dikes. Mostafa et al. (2023) studied the flow structure and velocity around hybrid groins affected by different angles and geometry orientations using ADV.

To understand the effect of the channel constriction due to the groins presence on flow characteristics, longitudinal and transverse velocity variations at the groins tip were investigated. Most of the previous works related to triangular vanes mainly considered the impermeable form of these structures and focused on the local scour characteristics, morphological changes, and bed deformations affected by the vanes spacing in the straight and meandering channel conditions. Detailed results about turbulent flow features have not been presented for these structures. In this paper, LES model is employed to understand the effect of different permeability rates and vanes angles on turbulent flow characteristics around these structures. LES model is used due to its capability of modelling the wakes and vortices more accurately.

2. Materials and Methods

2.1. Governing Equations

LES is a turbulent model applied in a wide variety of engineering applications in which by filtering the partial differential equations, continuity and Navier-Stokes equations for incompressible flows are written as follows:

$$\frac{\partial \overline{u_i}}{\partial x_i} = 0 \quad (1)$$

$$\frac{\partial \overline{u_i}}{\partial t} + \frac{\partial (\overline{u_i u_j})}{\partial x_j} = -\frac{1}{\rho}\frac{\partial \bar{p}}{\partial x_i} + 2v\frac{\partial}{\partial x_j}\overline{S_{ij}} \quad (2)$$

where $\overline{u_i}$: is the filtered velocity component x_i and x_j: are the spatial coordinate, t: is time variable, ρ: is fluid density, v: is kinematic viscosity, $\bar{p}$: is the filtered pressure field, $\overline{S_{ij}}$: is the rate-of-strain tensor, $\overline{u_i u_j}$: is a nonlinear filtered term which needs to be modeled since the unfiltered velocity field is unknown. The term can be split up, and the filtered Navier-Stokes equations are written as below:

$$\overline{u_i u_j} = \tau_{ij} + \overline{u_i}\overline{u_j} \quad (3)$$

$$\frac{\partial \overline{u_i}}{\partial t} + \frac{\partial (\overline{u_i}\overline{u_j})}{\partial x_j} = -\frac{\partial \bar{p}}{\rho\, \partial x_i} + 2v\frac{\partial}{\partial x_j}\overline{S_{ij}} - \frac{\partial \tau_{ij}}{\partial x_j} \quad (4)$$

Smagorinsky-Lilly subgrid-scale model was used to model the unclosed residual stress tensor τ_{ij}. Eddy-viscosity is modelled in this subgrid-scale model and the governing equations of Smagorinsky-Lilly model can be written as follows (Smagorinsky, 1963):

$$\tau_{ij} - \frac{1}{3}\tau_{kk}\delta_{ij} = -2\mu_t\overline{S_{ij}} \quad (5)$$

$$\mu_t = \rho(C_s\Delta)^2|\bar{S}| \quad (6)$$

$$\bar{S} = \sqrt{2S_{ij}S_{ij}} \quad (7)$$

where C_s, μ_t, ρ and Δ: are the model constant (0.1 - 0.2), eddy viscosity, density, and cube root of the local grid cell volume, respectively. τ_{kk}: is the isotropic part of the subgrid stresses, δ_{ij}: is kronecker delta and $|\bar{S}|$: is magnitude of the resolved strain-rate tensor.

2.2. Numerical Model

2.2.1. Model Setup

The computational domain composed of a rectangular channel and non-submerged triangular vanes of varying permeability rates and angles which was created and meshed using Gambit. Channel length (L) and width (B) were considered as 2 m and 0.5 m and contraction ratio (L_v / B) was 0.25, where L_v: is the length of the vane.

Cylindrical tubes of 6 mm diameter with different intervals were considered to adjust the different permeability rates (P) (Figure 1). Boundary conditions at the channel inlet, outlet, and solid surfaces, such as vanes, channel bed, and side walls were defined as pressure inlet, pressure outlet, and wall, respectively. For the free surface, a pressure inlet boundary condition was used.

Fluent was used to simulate turbulent flow around triangular vanes. Inlet flow depth (H), approach flow velocity (V_{app}), flow Froude and Reynolds numbers were 0.15, 0.66, 0.54, and 61875, respectively.

Stream wise distance from the vanes, transverse distance from the channel sidewall, and vertical distance from the channel bed are defined by X, Y, and Z, respectively. Negative and positive values refer to sections located upstream and downstream of the vanes.

2.2.2. Data Validation

In this paper, the results of the tip velocity (V_{tip}/V_{app}), flow separation angle ($\beta°$) and downstream flow separation width (W_S/B) of impermeable triangular groins of the experimental study of Kang et al. (2011) were used to evaluate the applied numerical model accuracy and determine the appropriate number of nodes. Numerical simulations were performed under the same conditions, except for channel length, which was reduced to 3 m to avoid large mesh numbers.

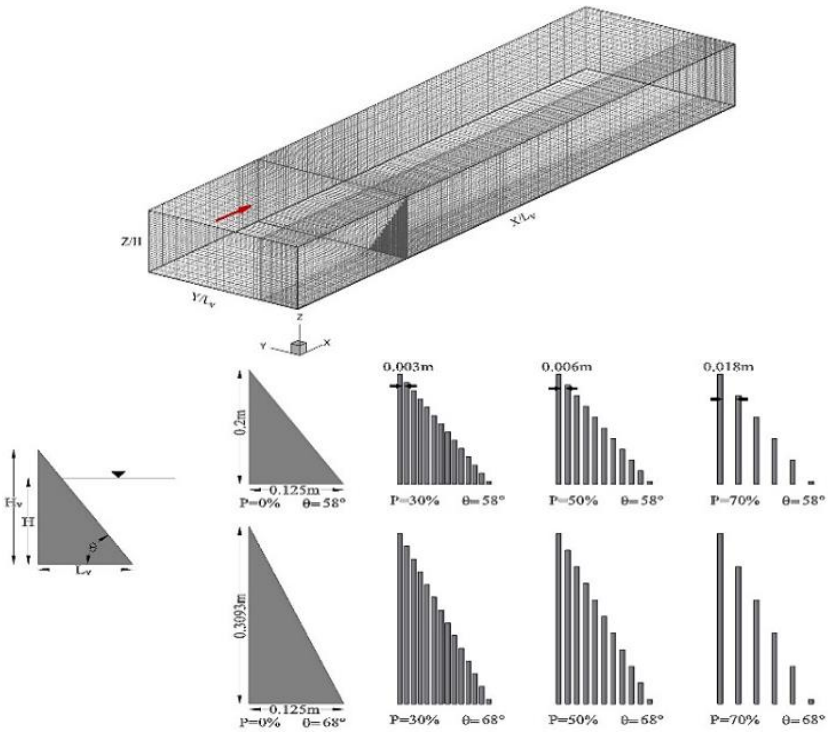

Fig. 1. Computational domain and dimensions of simulated vanes

Since the relative error values of the compared parameters are less than 10%, LES model can resolve the turbulent flow field accurately (Table 1). Furthermore, mesh independence test results for impermeable triangular groin (θ = 45°) showed a negligible difference (4.6%) between experimental and simulated values of the tip velocity by increasing the number of nodes; thus, a mesh composed of approximately 151400 to 170600 nodes was applied to all models (Figure 2).

3. Results and Discussions

3.1. Depth-Averaged Velocity

Velocity distribution in all simulated models clearly showed that due to the local effects of vanes' structure and channel constriction as a result of the vanes' protrusion, two zones are formed in the flow field, which are the main flow field, upstream, and downstream separation region (Figure 3).

These zones are separated by a fully turbulent and dynamic flow named detached shear layer. In the upstream of the impermeable vanes, $-1.6 \leq X/L_v \leq 0$, flow velocities near the channel side wall reduced due to the backwater effect. At the $X/L_v = 0$ section, local flow has been affected and velocity values have been increased due to the flow deflection. In the downstream region, presence of the recirculation zone, detached shear layer, different wakes and vortices significantly affected the flow field and maximum velocities occurred in this region. On average, maximum velocity values are $1.46V_{app}$.

Generally presence of the horseshoe vortices and high velocity zone near the bed and vanes tip region effects the local scour hole characteristics. Tip velocity in this critical region has a declining trend with increasing permeability rates and decreases up to 25% for the 70% permeable vane with θ = 58° and 31.8% in the θ = 68° case.

Table 1. Numerical simulation validation results

Crest angle (θ)	V_{tip} / V_{app}	β°	W_S / B
35	5.86%	6.25%	6.52%
45	4.6%	6.06%	6.66%

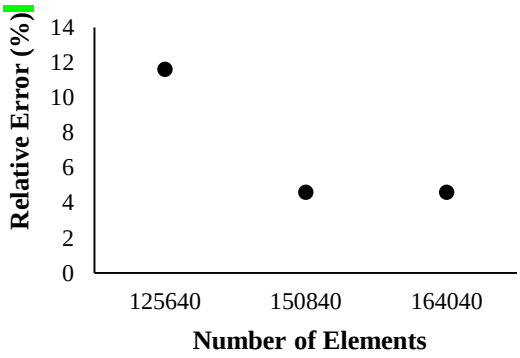

Fig. 2. Average relative error of experimental and simulated tip velocity of impermeable triangular groin (θ = 45°)

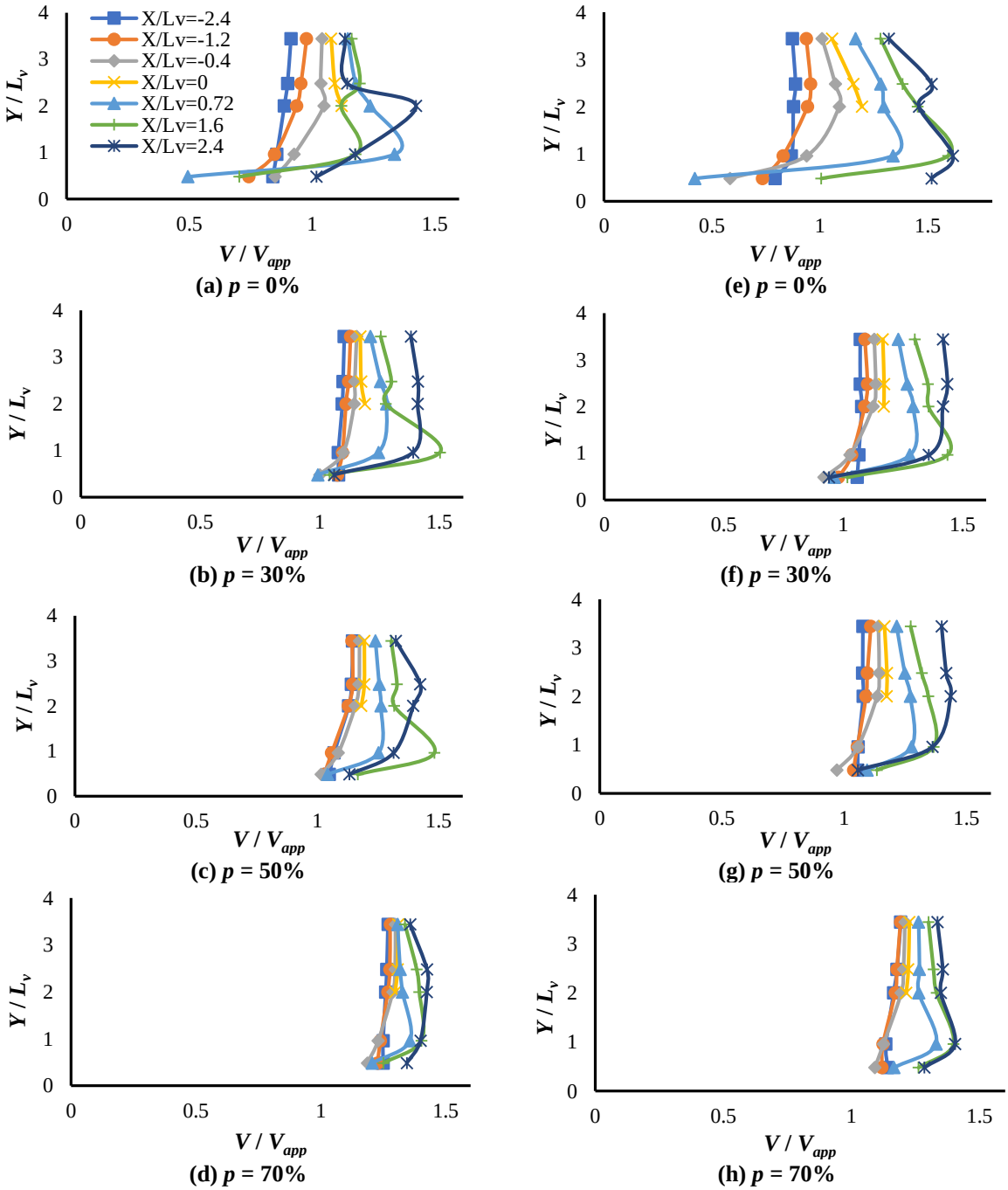

Fig. 3. Depth-averaged velocity distribution around triangular vanes; a, b, c, and d) θ = 58°; and e, f, g, and h) θ = 68°

3.2. Bed Shear Stress

In this study, bed shear stress variation around the triangular vanes is plotted using the dimensionless parameter (τ / τ_{Mean}), where τ_{Mean}: is the average bed shear stress of the impermeable rectangular vane at the channel entrance (Figure 4).

Generally, due to the complex condition of the downstream region, such as flow deflection within the different layers of the flow field, formation of the strong eddies, secondary flows within the recirculation zone, and their subsequent interaction with different wakes or vortices, maximum bed shear stress values mainly occurred at X / L_v = 2.4 section.

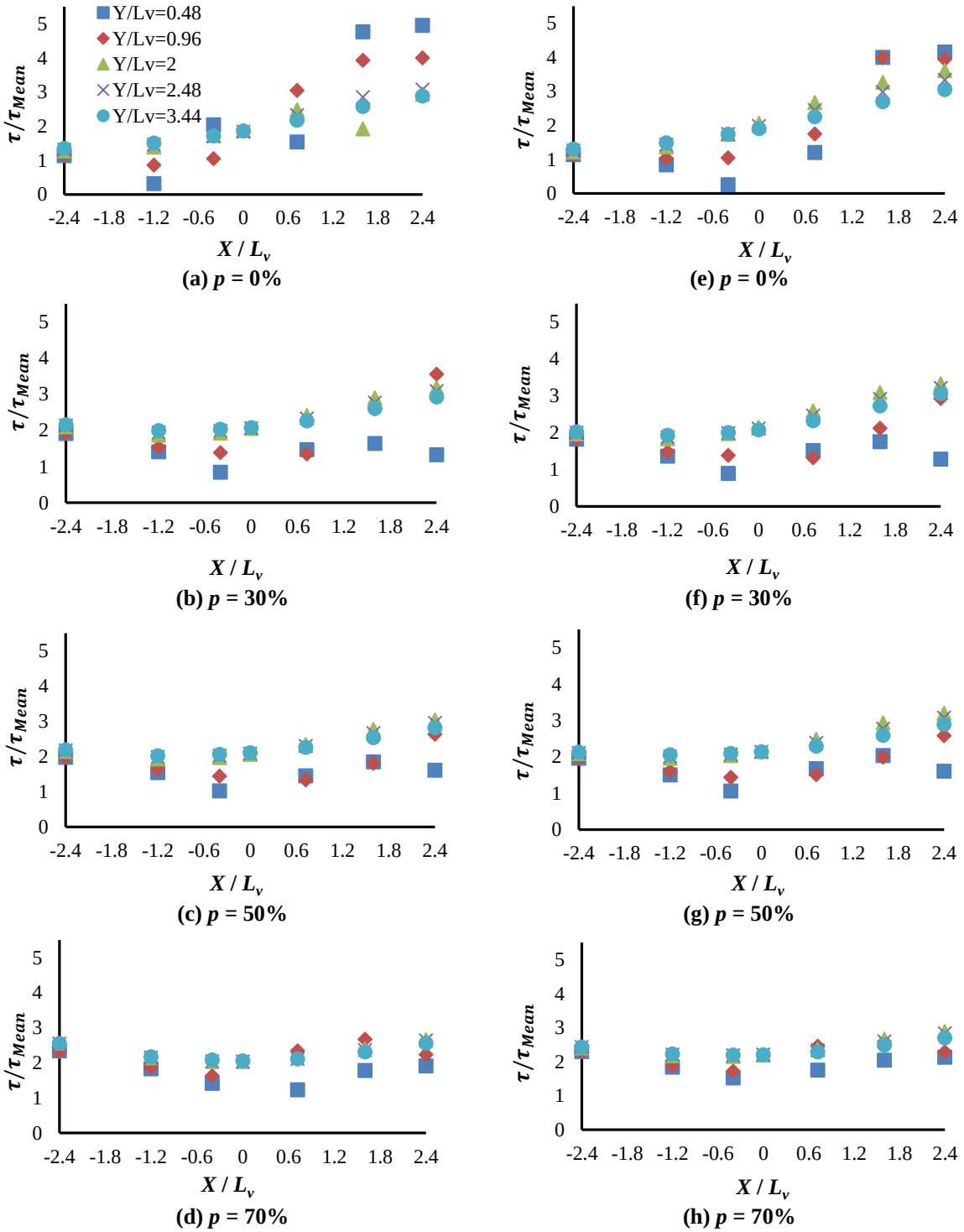

Fig. 4. Bed shear stress variations around simulated triangular vanes; a, b, c, and d) θ = 58°; and e, f, g, and h) θ = 68°

Maximum bed shear stress decreases up to 45.6% for the 70% permeable vane with θ = 58° and 30.3% in the θ = 68° case. Furthermore, maximum bed shear stress values shifted to the channel centreline by increasing the permeability rates of the triangular vane. Maximum values of the friction coefficient for all of the simulated triangular vanes vary between $0.006 \leq C_{fmax} \leq 0.018$ along the $-2.4 \leq X / L_v \leq 2.4$ region.

3.3. Thalweg Line Variation

The maximum stream wise velocity line, which is considered as the deepest flow line in alluvial rivers, is defined as the thalweg line. Upstream of the impermeable vanes, as flow reaches the vicinity of the structure, it begins to bend, and velocity magnitude values increase. The highest velocity values occur at the $X/L_v = 0$ section. In the downstream, as the vanes' presence impact on the main flow field decreases, the thalweg line gradually returns to the channel centerline. The main flow field constriction and local flow structure affected by the vanes' protrusion mainly deflect the thalweg line from the channel centerline. Generally, by increasing the permeability rate of the vanes, the downstream recirculation zone does not form due to the smaller flow deflection angles (Figure 5a); thus, for 70% permeable triangular vanes, the thalweg line is almost coincident with the channel centerline (Figures 5b and 5c).

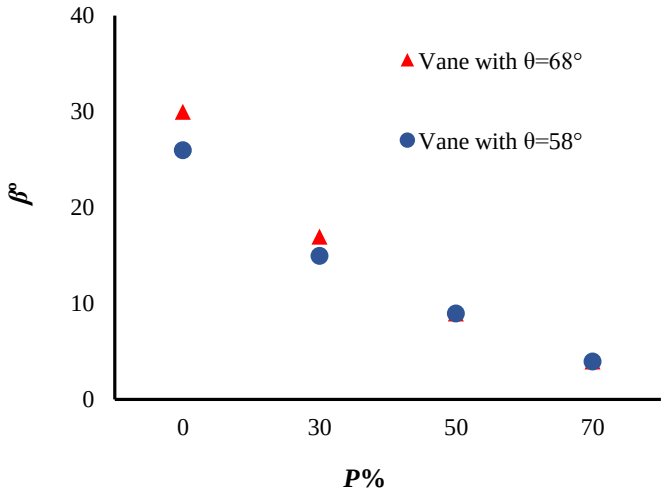

(a)

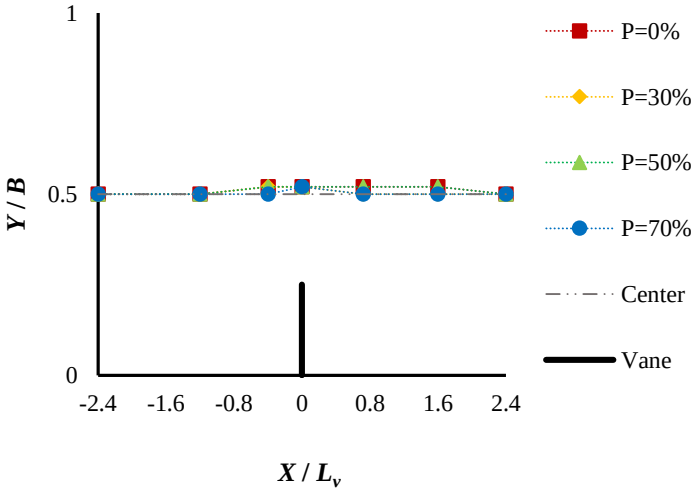

(b)

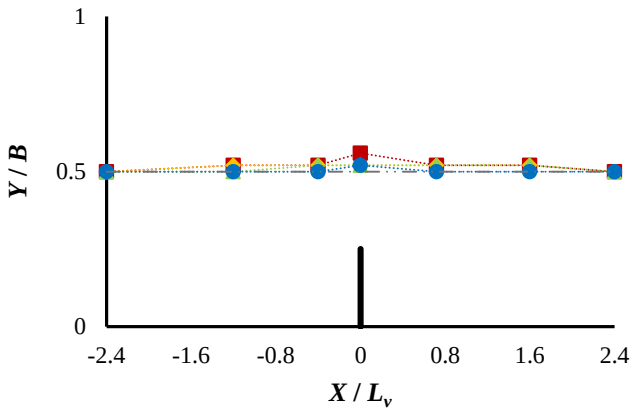

(c)

Fig. 5. Flow deflection angle and thalweg line variations; a) Flow deflection angle; b) θ = 58°; and c) θ = 68°

4. Conclusions

Numerical model accuracy assessed using experimental results of the tip velocity, flow separation angle, and downstream flow separation width of impermeable triangular groins of Kang et al. (2011) study.

The experimental and numerical results agreed well, since the average relative error values were less than 10%. Depth-averaged velocity distribution and bed shear stress variations showed that the presence of the impermeable triangular vanes significantly affected the downstream flow field due to the formation of the strong and stable vortices. Maximum velocities in all cases generally occurred in the $1.6 \leq X/L_v \leq 2.4$ region. Furthermore, at the near-bed region, tip velocity increased up to 10% for the impermeable triangular vane with θ = 68°.

Depth-averaged velocity variations clearly showed the presence of two different zones in the flow field, flow separation and turbulence due to the interaction of different wakes and vortices affected the flow velocities and sediment deposition process in these regions. Bed shear stress variation results showed that by increasing the vane angle from 58° to 68° in impermeable cases, maximum bed shear stress decreases up to 16.3%. Generally, for all simulated vanes, the maximum shear stress ratio (τ_{Max}/τ_{Mean}) varies between 2.6 and 4.9. Furthermore, maximum shear stress values shifted towards the channel centerline in permeable cases; thus, this could be considered as one of the advantages of these structures in comparison to the impermeable ones for the river bank protection. However, it must be noted that vanes with higher permeability rates do not have a noticeable effect on controlling the local flow characteristics and velocity decreasing. Channel lateral constriction reduced due to the triangular vanes' cross-sectional opening; thus, weaker vortices occurred in the flow field, and in all of the simulated cases, the thalweg line shifts closer to the channel centerline.

5. References

Abdou, S.S., ElMoustafa, A.M. and Samy, M. (2021). "Assessing flow bends in open channels", *International Research Journal of Advanced Engineering and Science*, 6(2), 49-54, http://irjaes.com/wp-content/uploads/2021/04/IRJAES-V6N2P55Y21.pdf.

Bahrami Yarahmadi, M. and Shafai Bejestan, M. (2015). "Sediment management and flow patterns at river bend due to triangular vanes attached to the bank", *Journal of Hydro-environment Research*, 10, 64-75, https://doi.org/10.1016/j.jher.2015.10.002.

Bhuiyan, F., Hey, R.D. and Wormleaton, P.R. (2010). "Bank-attached vanes for bank erosion control and restoration of river meanders", *Journal of Hydraulic Engineering*, 136(9), 583-596, https://doi.org/10.1061/(ASCE)HY.1943-7900.0000217.

Fang, H., Bai, J., He, G. and Zhao, H. (2014). "Calculations of nonsubmerged groin flow in a shallow open channel by large-eddy

simulation", *Journal of Engineering Mechanics*, 140(5), 04014016, https://doi.org/10.1061/(ASCE)EM.1943-7889.0000711.

Ferro, V., Shokrian Hajibehzad, M., Shafai Bejestan, M. and Kashefipour, S.M. (2019). "Scour around a permeable groin combined with a triangular vane in river bends", *Journal of Irrigation and Drainage Engineering*, 145(3), 04019003, https://doi.org/10.1061/(ASCE)IR.1943-4774.0001380.

Haider, R., Qiao, D., Yan, J., Ning, D., Ahmed Pasha, G. and Iqbal, S. (2022). "Flow characteristics around permeable spur dike with different staggered pores at varying angles", *Arabian Journal of Science and Engineering*, 47, 5219-5236, https://doi.org/10.1007/s13369-021-06435-4.

Iqbal, S., Pasha, G.A., Ghani, U., Ullah, M.K. and Ahmad, A. (2021). "Flow dynamics around permeable spur dike in a rectangular channel", *Arabian Journal for Science and Engineering*, 46, 4999-5011, https://doi.org/10.1007/s13369-020-05205-y.

Jafari, R. and Sui, J. (2021). "Velocity field and turbulence structure around spur dikes with different angles of orientation under ice covered flow conditions", *Water*, 13(13), 1844, https://doi.org/10.3390/w13131844.

Kang, J., Yeo, H., Kim, S. and Ji, U. (2011). "Permeability effects of single groin on flow characteristics", *Journal of Hydraulic Research*, 49(6), 728-735, https://doi.org/10.1080/00221686.2011.614520.

Mostafa, M.M., Ameen, M.A., Mohamed, H.I. and Ahmed, H.S. (2023). "Optimal flow pattern around hybrid groins with various orientations to improve fish habitat via experimental investigation using acoustic doppler velocimeter", *SVU-International Journal of Engineering Sciences and Applications*, 4(2), 98-106, https://doi.org/10.21608/svusrc.2023.189730.1096.

Pagliara, S. and Kurdistani, S.M. (2017). "Flume experiments on scour downstream of wood stream restoration structures", *Geomorphology*, 279(2), 141-149, https://doi.org/10.1016/j.geomorph.2016.10.013.

Shampa, S., Hasegawa, Y., Nakagawa, H., Takebayashi, H. and Kawaike, K. (2020). "Three-dimensional flow characteristics in slit-type permeable spur dike fields: Efficacy in riverbank protection", *Water*, 12(4), https://doi.org/10.3390/w12040964.

Smagorinsky, J. (1963). "General circulation experiments with the primitive equations I, the basic experiment", *Monthly Weather Review*, 91(3), 99-164.

Teraguchi, H., Nakagawa, H., Kawaike, K., Baba, Y. and Zhang, H. (2011). "Effects of hydraulic structures on river morphological process", *International Journal of Sediment Research*, 26(3), 283-303, https://doi.org/10.1016/S1001-6279(11)60094-2.

Wang, W., Liao, W. and Qi, L. (2020). "Experiment of turbulent characteristics of flow in wide and narrow Channels", *Advances in Water Science*, 31(3), 394-403, https://doi.org/10.14042/j.cnki.32.1309.2020.03.009.